

Neutrinophilic Λ CDM Extension for EMPRESS, DESI and Hubble Tension

Yuan-Zhen Li^{1, 2, *} and Jiang-Hao Yu^{1, 2, 3, †}

¹*CAS Key Laboratory of Theoretical Physics, Institute of Theoretical Physics,
Chinese Academy of Sciences, Beijing 100190, P. R. China*

²*School of Physical Sciences, University of Chinese Academy of Sciences, Beijing 100049, P. R. China*

³*School of Fundamental Physics and Mathematical Sciences,
Hangzhou Institute for Advanced Study, UCAS, Hangzhou 310024, China*

A number of recent cosmological observations have indicated the presence of new physics beyond the Λ CDM model. Combining observations from EMPRESS on helium abundance and DESI on baryon acoustic oscillations with Hubble tension, we show that all of them can be explained concurrently with a extension of the Λ CDM model with primordial neutrino asymmetry ξ_ν and additional contribution to the effective number of neutrinos δN_{eff} . Based on the accurate treatments of neutrino decoupling and BBN processes, we present state-of-the-art constraints on neutrino asymmetry for the fixed or varying N_{eff} . Comparing different extensions of the Λ CDM model, we show that the neutrinophilic Λ CDM extension with $\xi_\nu = 0.056 \pm 0.017$ and $\delta N_{\text{eff}} = 0.41 \pm 0.16$ is preferred by current observations, while the Hubble tension in this model is also alleviated to be 2.2σ .

Introduction. We are now in the era of precision cosmology, where observations of both the early and late universe provide key insights into beyond the Standard Model (SM) physics. Precision measurements of the Cosmic Microwave Background (CMB) over the past decade by Planck [1], ACT [2, 3], and SPT [4] are consistent with the Λ Cold Dark Matter (Λ CDM) model, which incorporates non-baryonic cold dark matter and dark energy as a cosmological constant, Λ [5–7]. However, recent data indicates possibility of new physics beyond the Λ CDM framework.

For late universe, the most notable indication is the "Hubble tension", where measurements of the Hubble constant from local distance ladders (using Cepheids and other anchors) differ from those obtained via CMB observations based on the Λ CDM model, at the $4 - 5\sigma$ level [1, 8–12]. This significant discrepancy between early and late universe observations suggests potential shortcomings in the Λ CDM model [13], leading to increased interest in recent years, see [14–17] for recent reviews on possible solutions. Moreover, observations from the Dark Energy Spectroscopic Instrument (DESI) collaboration also hints on possible cosmological scenarios beyond Λ CDM [18]. DESI measures the imprint of the sound horizon at the drag epoch, r_d , on galaxy, quasar, and Lyman α forest clustering, providing the strongest constraints to date on both the expansion history and growth rate of the Large Scale Structure (LSS). When combining DESI BAO data with CMB [1, 3] and PantheonPlus [19] (DESY5 [20]) data, the DESI collaboration finds that the dynamical dark energy model is favored over the Λ CDM model at the 2.5σ (3.9σ) significance level.

On the other hand, the recent EMPRESS survey of primordial elements from Big Bang Nucleosynthesis (BBN) in extremely metal-poor galaxies reports a primordial helium-4 determination of $Y_P = 0.2370^{+0.0034}_{-0.0033}$ [21], about 3σ deviation than the SM prediction [22]. Since proton-

neutron decoupling at the onset of BBN is influenced by electron neutrino properties, the EMPRESS result suggests a non-zero Primordial Neutrino Asymmetry (PNA) ξ_ν [21, 23–25]. However, previous analyses overlook several aspects: first, the effects of PNA on the neutrino decoupling process; second, the radiative and nucleon mass corrections to weak rates for accurate BBN predictions; third, the constraining power of BAO observations on PNA, although they are widely used to constrain neutrino properties like the sum of neutrino masses $\sum m_\nu$ and the effective number of neutrinos N_{eff} .

In this letter, we present the first detailed analysis on the implications of PNA by combining the EMPRESS BBN, CMB and DESI BAO observations, based on the accurate BBN predictions from the companion paper [26], which addresses the above three aspects with only the BOSS BAO data [27–29]. For both fixed and freely-varying N_{eff} , we present state-of-the-art constraints on PNA and discuss the implications of including LSS data. Surprisingly, we find that both the peculiar EMPRESS BBN and DESI BAO observations can be simultaneously explained by a simple neutrinophilic Λ CDM model with PNA ξ_ν and additional contribution to effective number of neutrinos δN_{eff} , while alleviating the Hubble tension to the 2.2σ level, although alternative models can explain each observation individually. This neutrinophilic Λ CDM model is also preferred over the $\omega_0\omega_a$ CDM model and other Λ CDM extensions.

Primordial Neutrino Asymmetry and implications. Primordial neutrino asymmetry is usually parameterised with the degeneracy parameters $\xi_{\nu_\alpha} \equiv \mu_{\nu_\alpha}/T_{\nu_\alpha}$ [30], defined as the chemical potential for the flavour α neutrino normalised to its temperature, so that

$$\eta_\nu \equiv \frac{1}{n_\gamma} \sum_{\alpha=e,\mu,\tau} (n_{\nu_\alpha} - n_{\bar{\nu}_\alpha}) \simeq \frac{\pi^2}{33\zeta(3)} \sum_{\alpha=e,\mu,\tau} \xi_{\nu_\alpha}, \quad (1)$$

where n_γ represents the photon number density, and n_{ν_α} ($n_{\bar{\nu}_\alpha}$) refers to the (anti)neutrino number density for

flavour α . In Eq. 1, the SM value for the neutrino-photon temperature ratio $T_{\nu_i}/T_\gamma = (4/11)^{1/3}$ and a small degeneracy $\xi_{\nu_\alpha} \ll 1$ are assumed, such that higher-order terms in ξ_{ν_α} can be neglected. Despite the sphaleron process in the early universe [31–34], various models can generate a PNA η_ν that is much larger than the baryon asymmetry of the universe $\eta_B \equiv n_B/n_\gamma \sim \mathcal{O}(10^{-10})$ [35–43].

During evolution of the universe, PNA induces significant changes in various epochs, including neutrino decoupling, BBN, CMB, and LSS formation. In the following, we will explore these effects in detail based on an accurate treatment of full neutrino transport during decoupling in the companion paper [26].

For neutrino decoupling, both N_{eff} and the neutrino spectral distortions are modified in the presence of PNA. In the flavour-equilibrated case, where $\xi_{\nu_e} = \xi_{\nu_\mu} = \xi_{\nu_\tau} = \xi_\nu$, and accounting for flavour oscillations, matter effects, finite-temperature QED (FTQED) corrections up to order $\mathcal{O}(e^3)$, and full neutrino-electron and neutrino-neutrino collision terms, we find that

$$N_{\text{eff}} = N_{\text{eff}}^{\text{SM}} + 3 \left(\frac{30}{7\pi^2} \xi_\nu^2 + \frac{15}{7\pi^4} \xi_\nu^4 \right) + 0.0102 \xi_\nu^2, \quad (2)$$

where $N_{\text{eff}}^{\text{SM}} = 3.0440$ is the resulting N_{eff} for the SM case [44–46], and the second (third) term represent the contribution from PNA in (beyond) the instantaneous decoupling limit. In addition, neutrinos and antineutrinos experience different dynamics in the presence of PNA, leading to different spectral distortions with respect to corresponding thermal distributions.

In the BBN epoch, PNA primarily affects the neutron-proton conversion process and the final neutron-proton ratio after decoupling. Including these, along with corrections to weak rates for neutron-proton conversion (such as zero and finite temperature radiative corrections, nucleon mass corrections, and spectral distortions of neutrinos and antineutrinos), we provide state-of-the-art predictions for BBN in [26], which will be used in the Markov Chain Monte Carlo (MCMC) analysis.

Since neutrinos decouple completely during the formation of the CMB and LSS, the effects of the PNA are primarily expressed through two indirect effects: (1) the altered helium abundance Y_P from BBN, and (2) changes in the expansion history due to the increased N_{eff} and the non-relativistic effects of massive neutrinos. For the CMB, the dominant effect arises from the first term, which modifies the tail of the CMB angular power spectrum through diffusion damping. The second term influences the matter-radiation equality, the last scattering epoch, and the BAO scale r_d , leaving imprints on the matter power spectrum and galaxy distributions [47].

In summary, the neutrino cosmology with non-zero PNA ξ_ν and δN_{eff} would modify the whole cosmological history of the ΛCDM model. In the following, we call the modified cosmology due to extensions of neutrino properties as "the neutrinoophilic ΛCDM model".

Methodology. We will utilize the following datasets for our cosmological analysis:

BBN: For helium abundance, we use the EMPRESS result $Y_P = 0.2370^{+0.0034}_{-0.0033}$ [21]. For deuterium abundance, we adopt the Particle Data Group (PDG)'s recommended value $10^5 \times D/\text{H} = 2.547 \pm 0.025$ [48].

CMB: We use data from Planck collaboration, including low- and high- ℓ TT, TE, EE spectra, and the reconstructed CMB lensing spectrum [1, 49, 50].

BAO: We adopt the latest DESI BAO measurements, which probe the sound horizon imprints at the drag epoch r_d in the LSS [18]. These measurements directly provide constraints on the transverse comoving distance $D_M(z)$ and the equivalent distance $D_H(z)$, or their combination $D_V(z)/r_d = (z D_M(z)^2 D_H(z))^{1/3}/r_d$ [51].

SN Ia: For a complementary probe of the expansion history, we adopt type Ia supernovae (SN Ia) data from the PantheonPlus compilation, which includes 1550 spectroscopically confirmed SN Ia in the redshift range $0.001 < z < 2.26$ [19].

Combining these datasets and corresponding likelihoods, we perform MCMC analyses with the `MontePython` engine [52, 53] and the modified `CLASS` code [54, 55], incorporating state-of-the-art predictions for Y_P and D/H discussed above. In particular, we consider two approaches to the treatment of thermonuclear reaction rates in BBN: the PRIMAT-driven approach [22, 56–63] and the NACRE II-driven approach [57, 64–66]. While both approaches yield nearly identical predictions for Y_P , the PRIMAT-driven method predicts a significantly smaller D/H due to differing nuclear rates for 10 key reactions in BBN [22, 23, 26].

For the MCMC run, we require convergence of all chains according to the Gelman-Rubin criterion, $R - 1 < 0.01$, and use `getDist` [67] to derive the constraints presented in this letter. We employ two information criteria for model comparison: the change in chi-squared relative to the ΛCDM model, $\Delta\chi^2 = \chi^2_{\text{Model}} - \chi^2_{\Lambda\text{CDM}}$, and the Deviance Information Criterion (DIC) [68], $\Delta\text{DIC} = \text{DIC}_{\text{Model}} - \text{DIC}_{\Lambda\text{CDM}}$ [69]. For both criteria, a lower value indicates a larger preference for the model over the ΛCDM model (see e.g., Table 1 of [70]).

Result A: State-of-the-art constraints on PNA.

The constraints on PNA derived from two cosmological datasets: the traditional "BBN + CMB" and the new "BBN + CMB + DESI BAO + SN Ia" data sets, which incorporate the LSS observations.

First, we consider the cosmological model $\Lambda\text{CDM} + \sum m_\nu + \xi_\nu$, where N_{eff} is fixed to the value in Eq. (2). For both the PRIMAT-driven and NACRE II-driven BBN predictions, the corresponding 68% bounds for ω_b and ξ_ν are shown in Table I, while the PRIMAT-driven 68%

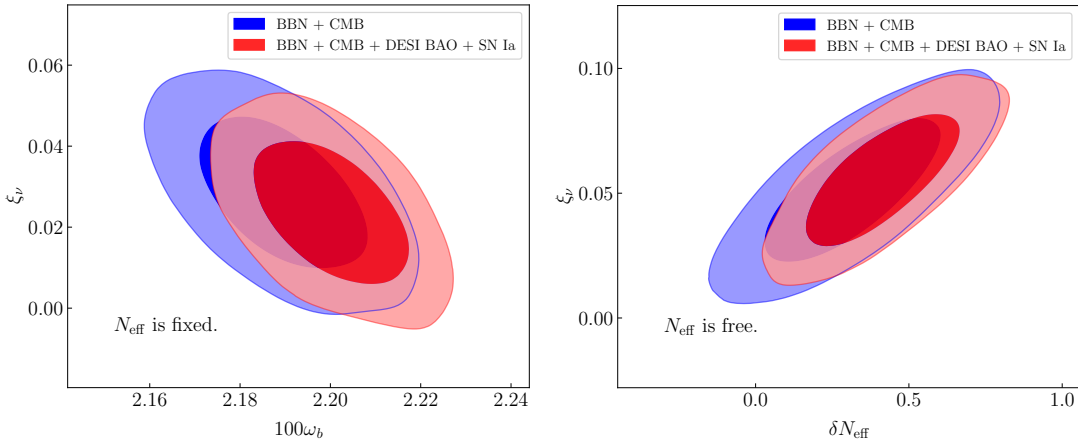


FIG. 1. Marginalized posterior distributions of the baryon abundance ω_b and the neutrino degeneracy parameter ξ_ν at the 68% and 95% confidence levels, obtained from a state-of-the-art analysis using the PRIMAT-driven approach for BBN prediction. The blue and red regions correspond to results derived from two different datasets of cosmological observations.

Bounds for the model: $\Lambda\text{CDM} + \sum m_\nu + \xi_\nu$						
Datasets	BBN Approach	ξ_ν	δN_{eff}	$\sum m_{\nu_i}$ (eV)	$100 \times \omega_b$	H_0 [km/s/Mpc]
BBN + CMB	PRIMAT	0.028 ± 0.012	—	0.40	2.190 ± 0.012	$65.1^{+1.6}_{-0.9}$
	NACRE II	0.034 ± 0.012	—	0.30	2.209 ± 0.012	$66.1^{+1.2}_{-0.65}$
BBN + CMB + DESI BAO + SN Ia	PRIMAT	0.024 ± 0.012	—	0.14	2.200 ± 0.011	66.99 ± 0.42
	NACRE II	0.031 ± 0.012	—	0.14	2.215 ± 0.011	67.23 ± 0.45
Bounds for the model: $\Lambda\text{CDM} + \sum m_\nu + \xi_\nu + \delta N_{\text{eff}}$						
Datasets	BBN Approach	ξ_ν	δN_{eff}	$\sum m_{\nu_i}$ (eV)	$100 \times \omega_b$	H_0 [km/s/Mpc]
BBN + CMB	PRIMAT	0.051 ± 0.018	0.31 ± 0.19	0.34	2.221 ± 0.023	$67.7^{+2.1}_{-1.7}$
	NACRE II	0.041 ± 0.019	0.08 ± 0.19	0.29	2.217 ± 0.022	$66.8^{+1.9}_{-1.6}$
BBN + CMB + DESI BAO + SN Ia	PRIMAT	0.056 ± 0.017	0.41 ± 0.16	0.16	2.236 ± 0.018	69.5 ± 1.2
	NACRE II	0.048 ± 0.018	0.20 ± 0.17	0.14	2.233 ± 0.018	68.6 ± 1.1

TABLE I. Summary of constraints for main parameters from considering several combinations of BBN, CMB, BAO and SN Ia data. See main text for details.

and 95% marginalized posteriors of ω_b and ξ_ν are shown in the left panel of Figure 1. For the "BBN + CMB" set, the constraints on ξ_ν are $\xi_\nu = 0.028 \pm 0.012$ for the PRIMAT driven approach and $\xi_\nu = 0.034 \pm 0.012$ for the NACRE II driven approach, with deviations of 2.3σ and 2.8σ from zero, respectively. Compared to previous results for the PRIMAT driven approach obtained in [24], our results show a $\sim 18\%$ smaller mean value and a slight reduce on uncertainty. With the LSS observation data, the resulting confidence region shifts towards a larger ω_b , and hence a smaller ξ_ν . Consequently, the bounds on ξ_ν become:

$$\xi_\nu = 0.024 \pm 0.012 \quad [\text{PRIMAT driven}], \quad (3)$$

$$\xi_\nu = 0.031 \pm 0.012 \quad [\text{NACRE II driven}], \quad (4)$$

where the significance of the deviations is reduced to 2.0σ and 2.6σ , respectively.

Allowing N_{eff} to vary freely significantly alters the constraints on ξ_ν and other parameters. As before, the resulting 68% confidence level constraints are summarized in Table I, while the PRIMAT-driven 68% and 95% confidence regions for δN_{eff} and ξ_ν are shown in the right panel of Figure 1. In general, allowing N_{eff} to vary freely increases both the central value and the uncertainties for the constraints on ξ_ν , while the constraints on δN_{eff} show significant variation depending on the assumed nuclear rates for BBN. For the "BBN + CMB" sets, the PRIMAT-driven approach yields a positive $\delta N_{\text{eff}} = 0.31 \pm 0.19$, whereas the NACRE II-driven approach gives $\delta N_{\text{eff}} = 0.08 \pm 0.19$, showing no significant preference [71]. More importantly, including the LSS observations in this analysis shifts the confidence region toward both a larger ξ_ν and a larger δN_{eff} . As a result, the constraints on ξ_ν and δN_{eff} for the NACRE

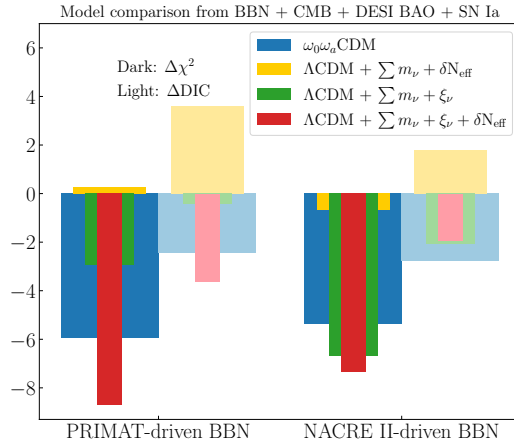


FIG. 2. Values of two information criteria, $\Delta\chi^2$ and ΔDIC for various models including the $\omega_0\omega_a$ CDM and neutrinoophilic Λ CDM extensions. A lower value indicate a larger preference for the model over the Λ CDM model.

II-driven approach are:

$$\xi_\nu = 0.048 \pm 0.018, \quad \delta N_{\text{eff}} = 0.20 \pm 0.17 \quad (5)$$

indicating a preference for a non-zero ξ_ν at the 2.7σ level and a non-zero δN_{eff} at the 1.2σ level. For the PRIMAT-driven approach, the constraints become:

$$\xi_\nu = 0.056 \pm 0.017, \quad \delta N_{\text{eff}} = 0.41 \pm 0.16 \quad (6)$$

with a preference for a non-zero ξ_ν at the 3.3σ level and a non-zero δN_{eff} at the 2.6σ level [72]. This preference for a non-zero δN_{eff} in both the BBN NACRE/PRIMAT-driven approaches arises from the need to fit the DESI BAO observations, and it also help alleviate the H_0 tension, as we will discuss later.

Result B: Model Comparison with EMPRESS and DESI. Using Λ CDM model as a benchmark, we will consider $\omega_0\omega_a$ CDM model and various neutrinoophilic Λ CDM extensions with ξ_ν or (and) δN_{eff} based on data from BBN, CMB, DESI BAO, and SN Ia. Values of the two information criteria we considered, $\Delta\chi^2$ and ΔDIC , are shown in Figure 2 with dark and light bars, respectively. For the $\omega_0\omega_a$ CDM model, both the PRIMAT-driven and NACRE II-driven approaches yield $\Delta\chi^2 \approx -6$ and $\Delta DIC \approx -2$, indicating a mild preference over Λ CDM, which is consistent with the finding in [18]. For the Λ CDM + $\sum m_\nu + \xi_\nu$ model, we see that the results depend on the BBN NACRE/PRIMAT-driven approaches, where the model performs better or similarly than the $\omega_0\omega_a$ CDM model based on the NACRE II-driven approach, while it performs worse based on the PRIMAT-driven approach. For the Λ CDM + $\sum m_\nu + \delta N_{\text{eff}}$ model, $\Delta\chi^2$ and ΔDIC are positive or nearly zero, showing an even worse performance than the Λ CDM model in both BBN approaches. Finally, we see that

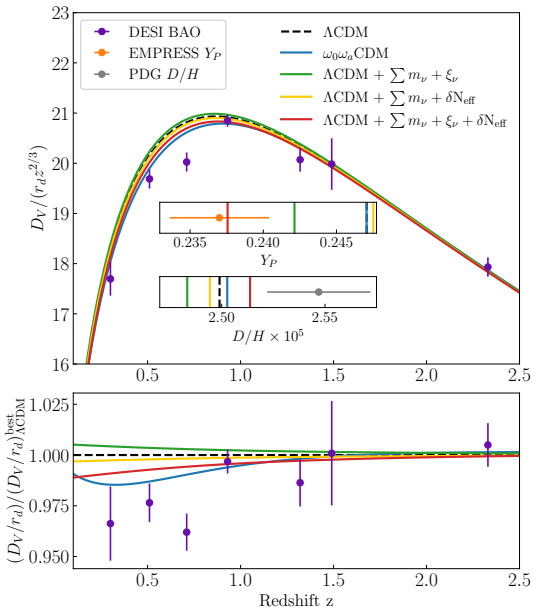


FIG. 3. Top panel: The DESI BAO results of the angle-averaged distance D_V/r_d normalized by $z^{-2/3}$ at various redshifts. The dashed and solid lines represent best-fit predictions from the Λ CDM model, $\omega_0\omega_a$ CDM model, and various neutrinoophilic Λ CDM extensions. The measurements of Y_P and D/H with the corresponding best-fit predictions are also included. Bottom panel: The same data points for DESI BAO and models as in the top panel, but normalized by the best-fit Λ CDM predictions.

the Λ CDM + $\sum m_\nu + \xi_\nu + \delta N_{\text{eff}}$ model yields a similar or smaller $\Delta\chi^2$ and ΔDIC in both BBN approaches, indicating a stronger preference over the $\omega_0\omega_a$ CDM [73].

To better understand the comparison results for these models, we show in Figure 3 the BBN and DESI BAO measurements, along with corresponding best-fit predictions from the Λ CDM, $\omega_0\omega_a$ CDM, and various neutrinoophilic Λ CDM extensions, based on the PRIMAT-driven approach for the BBN predictions. In the upper panel of Fig. 3, the DESI BAO measurements of the angle-averaged distance D_V/r_d at different redshifts are normalized by $z^{-2/3}$, while in the lower panel, they are normalized with the best-fit Λ CDM predictions. The BBN measurements and corresponding best-fit predictions are also included in the upper panel. Concerning the BBN measurements, we see that only the Λ CDM + $\sum m_\nu + \xi_\nu + \delta N_{\text{eff}}$ model can fit Y_P well while the D/H result roughly fits. The best-fits of all the other models cannot fit Y_P and D/H at the same time, which actually shows a slight tension between current Y_P and D/H measurements, see [26] for relevant discussions. Concerning the DESI BAO measurements, we find that while $\omega_0\omega_a$ CDM can fit the smaller D_V/r_d at low redshifts due to the modified late-time expansion, the Λ CDM + $\sum m_\nu + \xi_\nu + \delta N_{\text{eff}}$ model can also provide a satisfactory fit, which is caused by the positive δN_{eff} contributions

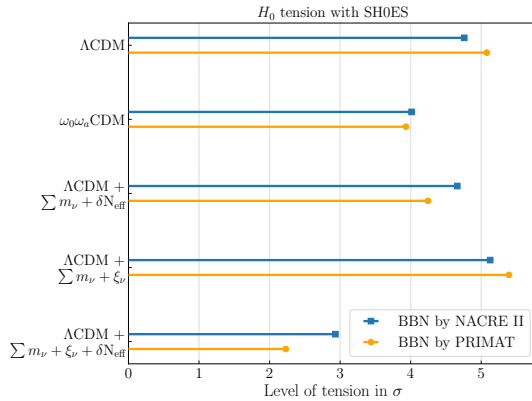


FIG. 4. A summary of the Hubble tension obtained from the combination of BBN, CMB, DESI BAO and SN Ia results and the SH0ES result of [12], assuming various cosmological models and approaches for BBN predictions.

needed to fit BBN measurements. In summary, only the $\Lambda\text{CDM} + \sum m_\nu + \xi_\nu + \delta N_{\text{eff}}$ model can fit both the BBN and DESI BAO observations well, which makes it the most preferred model.

Next we briefly discuss the results in the NACRE II-driven approach. Since the NACRE II-driven approach predicts a smaller D/H , both neutrinoophilic ΛCDM extensions with PNA can fit Y_P and D/H measurements well, leading to the preference of the $\Lambda\text{CDM} + \sum m_\nu + \xi_\nu$ model than the $\omega_0\omega_a\text{CDM}$ model in Figure 2. On the other hand, the best-fit of the $\Lambda\text{CDM} + \sum m_\nu + \xi_\nu + \delta N_{\text{eff}}$ model for the DESI BAO results becomes worse, as the late-time expansion history of the universe is less affected with the small δN_{eff} contribution in this case.

Result C: Alleviate the Hubble tension. For various cosmological models we considered, the results of Hubble parameter are summarized in Table I, while the significance of the Hubble tension compared to the SH0ES result [12] for both BBN nuclear approaches are shown in Figure 4. For both the ΛCDM model and its extensions with ξ_ν or δN_{eff} , the Hubble tension remains at $\sim 5\sigma$, while the $\omega_0\omega_a\text{CDM}$ model reduces it to $\sim 4\sigma$. However, for the $\Lambda\text{CDM} + \sum m_\nu + \xi_\nu + \delta N_{\text{eff}}$ model, the central value and uncertainties for the Hubble parameter both increase from the contribution of additional δN_{eff} . Consequently, Hubble tension is reduced to 2.2σ for the PRIMAT approach and 2.9σ for the NACRE II approach.

Summary and Outlook. Our study presents the first detailed analysis that combines attractive indications from EMPRESS BBN, DESI BAO measurements, and Hubble tension. While these are traditionally studied in detail individually, we show that a simple $\Lambda\text{CDM} + \sum m_\nu + \xi_\nu + \delta N_{\text{eff}}$ model can explain both the EMPRESS BBN and DESI BAO results, while reducing the Hubble tension to the 2.2σ level at the same time.

Along this direction, there are still many things to be discussed. First, we consider the S_8 tension, where

$S_8 = \sigma_8 \sqrt{\Omega_8/0.3}$, and σ_8 represents the amplitude of matter fluctuations on $8h^{-1}$ scales. Similar to the Hubble tension, the S_8 tension manifests as a $2 - 3\sigma$ discrepancy between early universe measurements and late universe cosmic shear data [74–82]. For our $\Lambda\text{CDM} + \sum m_\nu + \xi_\nu + \delta N_{\text{eff}}$ model, the MCMC analysis gives $S_8 = 0.840 \pm 0.011$ (PRIMAT-driven BBN) and $S_8 = 0.834 \pm 0.011$ (NACRE II-driven BBN), also showing a 3.0σ and 2.8σ tension with the DES-Y3 measurement [83], respectively.

We also note that the neutrino properties constraints are sensitive to the BBN observations. For instance, replacing the EMPRESS Y_P observation with the PDG value $Y_P = 0.2475 \pm 0.003$ [48] removes the preference for non-zero ξ_ν and δN_{eff} . As a result, the $\Lambda\text{CDM} + \sum m_\nu + \xi_\nu + \delta N_{\text{eff}}$ model no longer accommodates DESI BAO data or the Hubble tension. This highlights the critical role of accurate BBN measurements, which will remain an important probe of new physics in the future.

Acknowledgements. This work is supported by the National Science Foundation of China under Grants No. 12347105, No. 12375099 and No. 12047503, and the National Key Research and Development Program of China Grant No. 2020YFC2201501, No. 2021YFA0718304. The authors gratefully acknowledge the use of publicly available codes `FortEPiANO` [45, 84], `PRIMAT` [22], `CLASS` [54, 55], `MontePython` [52, 53] and `getDist` [67].

* liyuanzhen@itp.ac.cn

† jhyu@itp.ac.cn

- [1] N. Aghanim *et al.* (Planck), *Astron. Astrophys.* **641**, A6 (2020), [Erratum: *Astron. Astrophys.* 652, C4 (2021)], arXiv:1807.06209 [astro-ph.CO].
- [2] S. Aiola *et al.* (ACT), *JCAP* **12**, 047 (2020), arXiv:2007.07288 [astro-ph.CO].
- [3] M. S. Madhavacheril *et al.* (ACT), *Astrophys. J.* **962**, 113 (2024), arXiv:2304.05203 [astro-ph.CO].
- [4] D. Dutcher *et al.* (SPT-3G), *Phys. Rev. D* **104**, 022003 (2021), arXiv:2101.01684 [astro-ph.CO].
- [5] D. Baumann, D. Green, J. Meyers, and B. Wallisch, *JCAP* **01**, 007 (2016), arXiv:1508.06342 [astro-ph.CO].
- [6] E. Komatsu, *Nature Rev. Phys.* **4**, 452 (2022), arXiv:2202.13919 [astro-ph.CO].
- [7] C. L. Chang *et al.*, (2022), arXiv:2203.07638 [astro-ph.CO].
- [8] S. Alam *et al.* (eBOSS), *Phys. Rev. D* **103**, 083533 (2021), arXiv:2007.08991 [astro-ph.CO].
- [9] A. G. Riess *et al.*, *Astrophys. J.* **826**, 56 (2016), arXiv:1604.01424 [astro-ph.CO].
- [10] A. G. Riess *et al.*, *Astrophys. J.* **855**, 136 (2018), arXiv:1801.01120 [astro-ph.SR].
- [11] D. W. Pesce *et al.*, *Astrophys. J. Lett.* **891**, L1 (2020), arXiv:2001.09213 [astro-ph.CO].
- [12] A. G. Riess *et al.*, *Astrophys. J. Lett.* **934**, L7 (2022), arXiv:2112.04510 [astro-ph.CO].
- [13] Specifically, the SH0ES Cepheid-based distance ladder gives $H_0 = 73.04 \pm 1.04 \text{ km s}^{-1} \text{Mpc}^{-1}$ [12], while Planck reports $H_0 = 67.36 \pm 0.54 \text{ km s}^{-1} \text{Mpc}^{-1}$ based on the

Λ CDM model [1].

[14] L. Verde, T. Treu, and A. G. Riess, *Nature Astron.* **3**, 891 (2019), arXiv:1907.10625 [astro-ph.CO].

[15] E. Di Valentino et al., *Astropart. Phys.* **131**, 102605 (2021), arXiv:2008.11284 [astro-ph.CO].

[16] E. Di Valentino, O. Mena, S. Pan, L. Visinelli, W. Yang, A. Melchiorri, D. F. Mota, A. G. Riess, and J. Silk, *Class. Quant. Grav.* **38**, 153001 (2021), arXiv:2103.01183 [astro-ph.CO].

[17] M. Kamionkowski and A. G. Riess, *Ann. Rev. Nucl. Part. Sci.* **73**, 153 (2023), arXiv:2211.04492 [astro-ph.CO].

[18] A. G. Adame et al. (DESI), (2024), arXiv:2404.03002 [astro-ph.CO].

[19] D. Scolnic et al., *Astrophys. J.* **938**, 113 (2022), arXiv:2112.03863 [astro-ph.CO].

[20] T. M. C. Abbott et al. (Abbott, DES: T. M. C. DES), *Astrophys. J. Lett.* **973**, L14 (2024), arXiv:2401.02929 [astro-ph.CO].

[21] A. Matsumoto et al., *Astrophys. J.* **941**, 167 (2022), arXiv:2203.09617 [astro-ph.CO].

[22] C. Pitrou, A. Coc, J.-P. Uzan, and E. Vangioni, *Phys. Rept.* **754**, 1 (2018), arXiv:1801.08023 [astro-ph.CO].

[23] A.-K. Burns, T. M. P. Tait, and M. Valli, *Phys. Rev. Lett.* **130**, 131001 (2023), arXiv:2206.00693 [hep-ph].

[24] M. Escudero, A. Ibarra, and V. Maura, *Phys. Rev. D* **107**, 035024 (2023), arXiv:2208.03201 [hep-ph].

[25] J. Froustey and C. Pitrou, *Phys. Rev. D* **110**, 103551 (2024), arXiv:2405.06509 [hep-ph].

[26] Y.-Z. Li and J.-H. Yu, (2024), arXiv:2409.08280 [hep-ph].

[27] F. Beutler, C. Blake, M. Colless, D. H. Jones, L. Staveley-Smith, L. Campbell, Q. Parker, W. Saunders, and F. Watson, *Mon. Not. Roy. Astron. Soc.* **416**, 3017 (2011), arXiv:1106.3366 [astro-ph.CO].

[28] A. J. Ross, L. Samushia, C. Howlett, W. J. Percival, A. Burden, and M. Manera, *Mon. Not. Roy. Astron. Soc.* **449**, 835 (2015), arXiv:1409.3242 [astro-ph.CO].

[29] S. Alam et al. (BOSS), *Mon. Not. Roy. Astron. Soc.* **470**, 2617 (2017), arXiv:1607.03155 [astro-ph.CO].

[30] For sufficient large ξ_{ν_α} , the total lepton asymmetry is also dominated by the neutrino asymmetry, $\eta_L \simeq \eta_\nu$, due to the electric charge neutrality of the early universe.

[31] V. A. Kuzmin, V. A. Rubakov, and M. E. Shaposhnikov, *Phys. Lett. B* **155**, 36 (1985).

[32] S. Y. Khlebnikov and M. E. Shaposhnikov, *Nucl. Phys. B* **308**, 885 (1988).

[33] J. A. Harvey and M. S. Turner, *Phys. Rev. D* **42**, 3344 (1990).

[34] H. K. Dreiner and G. G. Ross, *Nucl. Phys. B* **410**, 188 (1993), arXiv:hep-ph/9207221.

[35] A. Casas, W. Y. Cheng, and G. Gelmini, *Nucl. Phys. B* **538**, 297 (1999), arXiv:hep-ph/9709289.

[36] A. D. Dolgov and D. P. Kirilova, *Sov. J. Nucl. Phys.* **51**, 172 (1990).

[37] B. Bajc, A. Riotto, and G. Senjanovic, *Phys. Rev. Lett.* **81**, 1355 (1998), arXiv:hep-ph/9710415.

[38] T. Asaka and M. Shaposhnikov, *Phys. Lett. B* **620**, 17 (2005), arXiv:hep-ph/0505013.

[39] T. Asaka, S. Blanchet, and M. Shaposhnikov, *Phys. Lett. B* **631**, 151 (2005), arXiv:hep-ph/0503065.

[40] A. Pilaftsis and T. E. J. Underwood, *Nucl. Phys. B* **692**, 303 (2004), arXiv:hep-ph/0309342.

[41] D. Borah and A. Dasgupta, *Phys. Rev. D* **108**, 035015 (2023), arXiv:2206.14722 [hep-ph].

[42] M. Kawasaki, F. Takahashi, and M. Yamaguchi, *Phys. Rev. D* **66**, 043516 (2002), arXiv:hep-ph/0205101.

[43] M. Kawasaki and K. Murai, *JCAP* **08**, 041 (2022), arXiv:2203.09713 [hep-ph].

[44] J. Froustey, C. Pitrou, and M. C. Volpe, *JCAP* **12**, 015 (2020), arXiv:2008.01074 [hep-ph].

[45] J. J. Bennett, G. Buldgen, P. F. De Salas, M. Drewes, S. Gariazzo, S. Pastor, and Y. Y. Y. Wong, *JCAP* **04**, 073 (2021), arXiv:2012.02726 [hep-ph].

[46] K. Akita and M. Yamaguchi, *JCAP* **08**, 012 (2020), arXiv:2005.07047 [hep-ph].

[47] Additionally, the free-streaming effect of massive neutrinos is also enhanced due to the increased neutrino momentum from the PNA, resulting in greater suppression of the matter power spectrum at small scales. However, this effect is nearly negligible compared to the impact of neutrino masses. See [26] for more details.

[48] R. L. Workman and Others (Particle Data Group), *PTEP* **2022**, 083C01 (2022).

[49] N. Aghanim et al. (Planck), *Astron. Astrophys.* **641**, A8 (2020), arXiv:1807.06210 [astro-ph.CO].

[50] N. Aghanim et al. (Planck), *Astron. Astrophys.* **641**, A5 (2020), arXiv:1907.12875 [astro-ph.CO].

[51] $D_M(z)$ is defined as $D_M(z) = \frac{c}{H_0\sqrt{\Omega_k}} \sinh \left[\sqrt{\Omega_k} \int_0^z \frac{dz'}{H(z')/H_0} \right]$, and $D_H(z)$ is defined as $D_H(z) = c/H(z)$. The constraints on these ratios at different redshifts are detailed in Tab. 1 of [18].

[52] B. Audren, J. Lesgourgues, K. Benabed, and S. Prunet, *JCAP* **02**, 001 (2013), arXiv:1210.7183 [astro-ph.CO].

[53] T. Brinckmann and J. Lesgourgues, *Phys. Dark Univ.* **24**, 100260 (2019), arXiv:1804.07261 [astro-ph.CO].

[54] J. Lesgourgues, (2011), arXiv:1104.2932 [astro-ph.IM].

[55] J. Lesgourgues and T. Tram, *JCAP* **09**, 032 (2011), arXiv:1104.2935 [astro-ph.CO].

[56] P. Descouvemont, A. Adahchour, C. Angulo, A. Coc, and E. Vangioni-Flam, *Atom. Data Nucl. Data Tabl.* **88**, 203 (2004), arXiv:astro-ph/0407101.

[57] C. Iliadis, K. Anderson, A. Coc, F. Timmes, and S. Starfield, *Astrophys. J.* **831**, 107 (2016), arXiv:1608.05853 [astro-ph.SR].

[58] A. Iñesta Gómez, C. Iliadis, and A. Coc, *Astrophys. J.* **849**, 134 (2017), arXiv:1710.01647 [astro-ph.IM].

[59] R. S. de Souza, C. Iliadis, and A. Coc, *Astrophys. J.* **872**, 75 (2019), arXiv:1809.06966 [astro-ph.IM].

[60] R. S. de Souza, S. R. Boston, A. Coc, and C. Iliadis, *Phys. Rev. C* **99**, 014619 (2019), arXiv:1901.04857 [nucl-th].

[61] J. Moscoso, R. S. de Souza, A. Coc, and C. Iliadis, *Astrophys. J.* **923**, 49 (2021), arXiv:2109.00049 [astro-ph.CO].

[62] C. Pitrou, A. Coc, J.-P. Uzan, and E. Vangioni, *Mon. Not. Roy. Astron. Soc.* **502**, 2474 (2021), arXiv:2011.11320 [astro-ph.CO].

[63] C. Pitrou, A. Coc, J.-P. Uzan, and E. Vangioni, *Nature Rev. Phys.* **3**, 231 (2021), arXiv:2104.11148 [astro-ph.CO].

[64] Y. Xu, K. Takahashi, S. Goriely, M. Arnould, M. Ohta, and H. Utsunomiya, *Nucl. Phys. A* **918**, 61 (2013), arXiv:1310.7099 [nucl-th].

[65] V. Mossa et al., *Nature* **587**, 210 (2020).

[66] B. D. Fields, K. A. Olive, T.-H. Yeh, and C. Young, *JCAP* **03**, 010 (2020), [Erratum: *JCAP* 11, E02 (2020)], arXiv:1912.01132 [astro-ph.CO].

[67] A. Lewis, (2019), arXiv:1910.13970 [astro-ph.IM].

[68] A. R. Liddle, *Mon. Not. Roy. Astron. Soc.* **377**, L74 (2007), arXiv:astro-ph/0701113.

[69] DIC is defined $DIC \equiv \langle \chi^2 \rangle + p_D$, where p_D is the effective number of parameters estimated from the posterior variance of the deviance, such that $p_D \equiv \langle \chi^2 \rangle - \chi^2(\langle \theta \rangle)$.

[70] S. Grandis, D. Rapetti, A. Saro, J. J. Mohr, and J. P. Dietrich, *Mon. Not. Roy. Astron. Soc.* **463**, 1416 (2016), arXiv:1604.06463 [astro-ph.CO].

[71] Compared to the results obtained in [24] with the PRIMAT approach, our analysis gives an almost identical central value with a slight reduction of the uncertainty for ξ_ν , while the preference for positive δN_{eff} is more significant in our analysis.

[72] It is worth noting that the required positive δN_{eff} cannot be fully explained by the contribution of ξ_ν under the assumption of flavor equilibration ($\xi_{\nu_e} = \xi_{\nu_\mu} = \xi_{\nu_\tau} = \xi_\nu$). However, it may be interpreted as the result of a large neutrino asymmetry in the muon-tau sector in the case where flavor equilibration is not fully realized, as discussed in the recent study [25].

[73] For the NACRE II-driven approach, the ΔDIC criterion shows a less preference of the $\Lambda\text{CDM} + \sum m_\nu + \xi_\nu + \delta N_{\text{eff}}$ model than the $\omega_0\omega_a\text{CDM}$ model, which is mainly caused by the fact that ΔDIC criterion particularly favors models with much less parameters.

[74] T. M. C. Abbott et al. (DES), *Phys. Rev. D* **105**, 023520 (2022), arXiv:2105.13549 [astro-ph.CO].

[75] E. Di Valentino et al., *Astropart. Phys.* **131**, 102604 (2021), arXiv:2008.11285 [astro-ph.CO].

[76] E. Di Valentino and S. Bridle, *Symmetry* **10**, 585 (2018).

[77] T. M. C. Abbott et al. (Kilo-Degree Survey, DES), *Open J. Astrophys.* **6**, 2305.17173 (2023), arXiv:2305.17173 [astro-ph.CO].

[78] T. Tröster et al., *Astron. Astrophys.* **633**, L10 (2020), arXiv:1909.11006 [astro-ph.CO].

[79] C. Heymans et al., *Astron. Astrophys.* **646**, A140 (2021), arXiv:2007.15632 [astro-ph.CO].

[80] R. Dalal et al., *Phys. Rev. D* **108**, 123519 (2023), arXiv:2304.00701 [astro-ph.CO].

[81] J. Kim et al., *JCAP* **12**, 022 (2024), arXiv:2407.04606 [astro-ph.CO].

[82] L. Faga et al. (DES), (2024), arXiv:2406.12675 [astro-ph.CO].

[83] A. Amon et al. (DES), *Phys. Rev. D* **105**, 023514 (2022), arXiv:2105.13543 [astro-ph.CO].

[84] S. Gariazzo, P. F. de Salas, and S. Pastor, *JCAP* **07**, 014 (2019), arXiv:1905.11290 [astro-ph.CO].